A High Resolution Optical Satellite Image Dataset for Ship Recognition and Some New Baselines

Zikun Liu[1,2], Liu Yuan[3], Lubin Weng[1] and Yiping Yang[1]

[1]*Institute of Automation Chinese Academy of Sciences, 95 Zhongguancun East Road, 100190, Beijing, China*
[2]*University of Chinese Academy of Sciences, 80 Zhongguancun East Road, 100190, Beijing, China*
[3]*China Academy of Electronics and Information Technology, 11 Shuanyuan Road, 100041, Beijing, China*
{*liuzikun2012, lubin.weng, yiping.yang*}*@ia.ac.cn, lyuan@csdslab.net*

Keywords: High Resolution Optical Remote Sensing Image, Sea-land Segmentation, Ship Detection, Ship Recognition, Dataset.

Abstract: Ship recognition in high-resolution optical satellite images is an important task. However, it is difficult to recognize ships under complex backgrounds, which is the main bottleneck for ship recognition and needs to be further explored and researched. As far as we know, there is no public remote sensing ship dataset and few open source work. To facilitate future ship recognition related research, in this paper, we present a public high-resolution ship dataset, "HRSC2016", that covers not only bounding-box labeling way, but also rotated bounding box way with three-level classes including ship, ship category and ship types. We also provide the ship head position for all the ships with "V" shape heads and the segmentation mask for every image in "Test set". Besides, we volunteer a ship annotation tool and some development tools. Given these rich annotations we perform a detailed analysis of some state-of-the-art methods, introduce a novel metric, the separation fitness (SF), that is used for evaluating the performance of the sea-land segmentation task and we also build some new baselines for recognition. The latest dataset can be downloaded from "http://www.escience.cn/people/liuzikun/DataSet.html".

1 INTRODUCTION

In the past decade, many countries have launched more and more satellites. We have entered an era of big data in remote sensing domain (Liu, 2015). We can now easily collect massive high-resolution remote sensing imageries.

With the progress of image's resolution and a rich supply of data, ship recognition from remote sensing imagery is becoming more and more important. There are a wide array of ship recognition related applications including fishery management, smuggling activities, vessel traffic services and naval warfare (Proia and Page, 2010; Zhu et al., 2010). Especially, due to political interest in security, maritime and docks surveillance has been highly prized. Ship monitoring by the way of remote sensing has some advantages such as a long operating distance and a wide monitoring range (Proia and Page, 2010).

Synthetic aperture radar (SAR) image data is the main data source for ship recognition and the optical remote sensing image is the helpful complement which is becoming more and more important, espe-

cially for ship recognition and accurate ship location . Many existing ship detection related works are based on SAR images, because SAR can work on day and night and can also resist interferences from clouds or some other factors. However, with the long term development of the optical remote sensing technique, the optical imagery can provide more details that is very important to be used to locate ships precisely and recognize ship types. At the same time, compared with SAR images, the interpretation results of optical images have also made information more intuitive to a human decision maker.

Most of the existing works are based on private dataset. The data sources include SPOT-5 (Corbane and Petit, 2008; Corbane et al., 2010; Proia and Page, 2010; Yang et al., 2014; Tang et al., 2015), WorldView-2 (Yokoya and Iwasaki, 2015), Quickbird (Liu et al., 2014), Venezuelan Remote Sensing Satellite (VRSS-1) (Zou and Shi, 2016), GaoFen-1 (GF-1) (Qi et al., 2015; Zou and Shi, 2016) and Google Earth (Guo et al., 2014; Shi et al., 2014; Xu et al., 2014; Yang et al., 2014; Qi et al., 2015; Yu et al., 2015; Zhang et al., 2016; Zou and Shi,
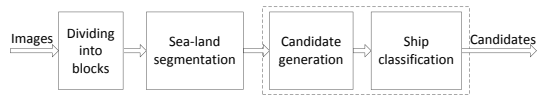
Figure 1: The four stages of ship recognition.

2016). The space resolution of the data from these data sources are about 5-m, 0.5-m, 0.61-m, 2.5-m, 2-m and 5m-0.4m respectively. Because of containing sensing data or copyrights, many private ship datasets are difficult to be publicly available. Yang et al. (Yang and Newsam, 2010) introduced a public dataset "LULC", which contains some overhead ship images collected from the United States Geological Survey National Map. However, "LULC" is used for land-use classification. High-resolution overhead imageries from Google Earth, which are publicly available for academic research, are collected by Landsat-7, QuickBird, IKONOS and SPOT-5, etc. Now, we plan to further build an open project for ship recognition based on images from Google Earth, which can be seen on our website. As far as we know, our dataset is the first unconcealed ground truth collection for ship recognition derived from publicly available high-resolution overhead imagery. Liu et al. (Liu et al., 2016) had done some experiments on our dataset.

Experiments on ship images derived from Google Earth are important references to practical applications with optical data directly collected from space-borne devices. Besides many existing works only based on images from Google Earth, some researchers performed experiments on both Google Earth images and the ones directly derived from satellites. For example, Zou et al. (Zou and Shi, 2016) used images from different data sources including Google Earth to train their SVD Networks and got much better classification performance by adding Google samples. Han et al. (Han et al., 2015) compared different methods on Google dataset and other datasets and gained similar performance differences between these methods.

Ship recognition can be divided into 4 stages demonstrated in Figure. 1. In the first stage, a large volume image is divided into small blocks laid to overlap each other which will be computed independently in the stages followed. However, this is not an indispensable step if the computing resource is not limited. The second stage is sea-land segmentation (You and Li, 2011; Liu et al., 2014; Tang et al., 2015), that is designed to speed up computing and help to extract ships. In the third stage, ship candidates with a lot of false alarms are proposed. And the fourth stage includes feature extraction, classification and non-maximal suppression (NMS). Most of the existing works covered both the third and fourth
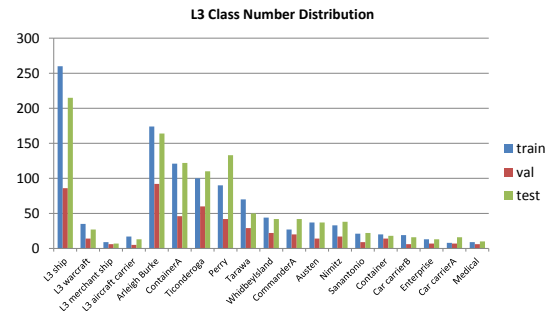

Figure 2: The level 3 class number distribution.

stage (Liu et al., 2014; Yu et al., 2015; Zhang et al., 2016; Zou and Shi, 2016). Liu et al. (Liu et al., 2016) proposed a method of candidate generation only with stage III. It is worth noting that Zou et al. (Zou and Shi, 2016) performed ship candidate generation and classification using one unified end-to-end training model which will be the future tendency.

However, due to lack of public dataset, it is difficult to compare different methods directly. Especially in sea-land segmentation task, the authors of existing works performed comparison on private dataset by visual inspection. Furthermore, very few public ship classification works explored ship type recognition which is an important task in naval warfare application. In fact, sub-class recognition is not uncommon in natural image domain (Yang et al., 2015).

The goal of our work is to promote the development of optical remote sensing ship recognition. In this paper, we build a standard public dataset with four unique features for ship recognition task, provide helping tools, analyze some state-of-the-art methods, propose a metric to evaluate the performance of sea-land segmentation and introduce a few new baselines.

2 HRSC2016

We call our dataset "High Resolution Ship Collection 2016" (HRSC2016). In section. 1, we have already introduced the demand of building a public optical remote sensing ship dataset and the important reference value of images derived from Google Earth. In this section, we describe the details of our dataset.

2.1 Dataset Setup

The HRSC2016 dataset contains images from two scenarios including ships on sea and ships close inshore. All the images are collected from six famous harbors. We not only collect the default images shown by Google Earth, but also download the history im-
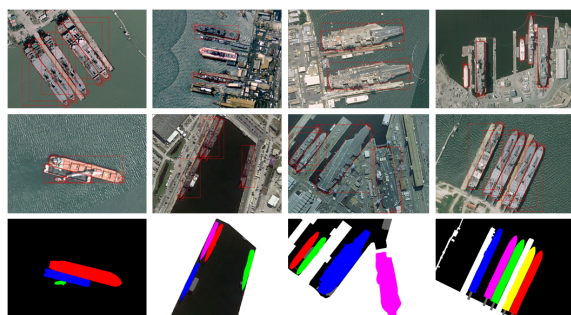
Figure 3: HRSC2016 samples. Training samples, test samples and segmentation masks are displayed in the first, second and third rows respectively. Each sample in HRSC2016 is annotated with bounding box, rotated bounding box and ship head location.

ages in the same place. The image resolutions are between 2-m and 0.4-m. The image sizes range from 300×300 to 1500×900 and most of them are larger than 1000×600.

In the process of collecting data, we recorded the image information including harbor, data source, image date, geographic coordinate, resolution layer, scale, etc. It is worth noting that Google Earth's geographic coordinate system may assign slightly different coordinates to the same location on the earth. And we just recorded a near geographic coordinate for each image.

We get 1061 images including 70 sea images with 90 samples and 991 sea-land images with 2886 samples. After adding annotations to these samples, we split the dataset into training, validation and test set which contains 436 images including 1207 samples, 181 images including 541 samples and 444 images including 1228 samples respectively.

Most of the HRSC2016 dataset images are inshore data. In order to satisfy the needs of the works for ship detection on sea, we provide another 610 images from Mumansk harbor, including 156 sea images and 454 sea-land images but without annotations. In the future, we will further extend our dataset.

2.2 Properties of HRSC2016

The HRSC2016 dataset has four unique features in comparison to existing private ship datasets, namely ship hierarchy, an abundance of bounding information, unbiasedness and rich helping tools.

2.2.1 Ship Hierarchy

In most of existing ship recognition related works, the candidates were only categorized into background or ship. Guo et al. (Guo et al., 2014) tried to divide ships into six sub-classes. However, it is still
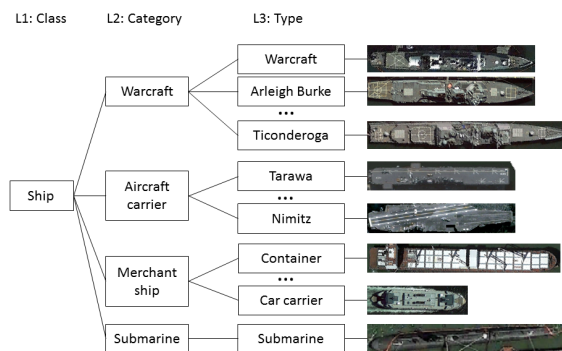

Figure 4: Ship model hierarchy. In the third level, ships with unknown types are marked by level 2 class.

in a coarse-grained level. In HRSC2016 dataset, the ship models are organized into a tree structure, consisting of three levels, namely ship class, ship category and ship type, as can be seen in Figure 4. In level three, ships with unknown types (the ones outside HRSC2016 ship type table) are marked by level 2 label. In the ship recognition task, we should recognize the right label in the tree as deeply as we possibly can.

2.2.2 An Abundance of Bounding Information

Ships with various rotation angles in optical remote sensing images are different from objects, most of which are stand-alone, in natural pictures. Because of bar-like objects, they are also different from other classical objects in optical remote sensing images, such as planes, cars, etc. It is not enough to only label ships by bounding box commonly used. Many existing works based on bounding box (Tang et al., 2015; Zou and Shi, 2016) are difficult to deal with ships in a cluster, as can be seen in Figure 3. Gan et al. (Gan et al., 2015) explored the rotation sliding box for ship detection. Liu et al. (Liu et al., 2016) proposed ship rotated bounding box space which is effective for extracting ships from complex backgrounds. In the future, there is a tendency to detect ships by machine learning methods based on rotated bounding box.

In HRSC2016 dataset, we provide three kinds of bounding information, namely bounding box, rotated bounding box and pixel-based segmentation, as can be seen in Figure 3. However, currently, we only provide segmentation masks for test set to evaluate algorithms. Furthermore, some existing methods (Liu et al., 2014) detected ships by locating ship heads. These part-detector based methods are very promising. In HRSC2016, we also provide ship head location information for all the ships with "V" shape heads.

2.2.3 Unbiasedness

In the world, the number of samples per ship type varies hugely. When we collected data, we downloaded the image with a random rotation angle if only it contains any ship. So the distribution of ship number in HRSC2016 reflects the real distribution, as can be seen in Figure 2. There are only 2976 samples for more than 25 ship classes. Several ship types come with only 1 to 20 samples in the dataset. Because of this, our dataset looks like the dataset of "Right Whale Recognition" for identifying endangered right whales on Kaggle's open data platform[1]. But our dataset is more complicated because there are always many ships in one image. It is not suitable to split all the images directly into training-validation and test set. In fact, we do this work using Algorithm 1 and get good result seen in Section 2.1 and Figure 2. We get training and validation set in the same way.

Algorithm 1: Splitting dataset algorithm.

Require:
    The set of ship classes, C;
    The set of ship samples, O;
    The set of images, I;

Ensure:
    The set of splitting result for each image in I;
1: Ordering C by "level" descending;
2: **for** each $c \in C$ **do**
3:    Finding samples (O_c) belong to c;
4:    **for** each $o \in O_c$ **do**
5:      Getting the image (i) that o belongs to;
6:      **if** i has been labeled **then**
7:        continue;
8:      **end if**
9:      Getting a random number r between $[0,1]$;
10:     **if** $r > 0.6$ **then**
11:       Labeling i as test image;
12:     **else**
13:       Labeling i as train-val image;
14:     **end if**
15:    **end for**
16: **end for**

2.2.4 Rich Helping Tools

We provide a development toolkit including an annotation tool, a database tool and some development tools. Currently, the annotation tool, shown in Figure. 5, only works in local host. In fact, the annotation work for ships needs professional knowledge. It is difficult for us to recognize all kinds of ship types in
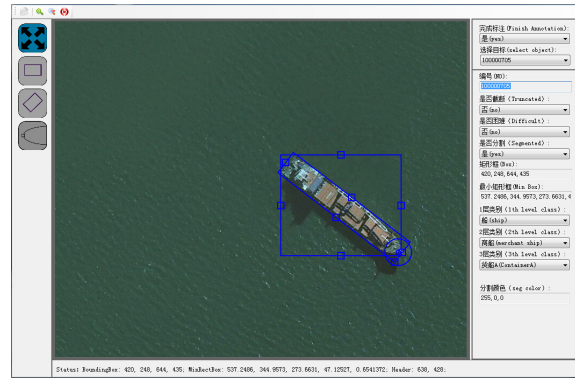

Figure 5: The annotation tool.

HRSC2016. The cost of finding an expert is too high to us. Inspired by Van Horn et al. (Van Horn et al., 2015), we plan to seek help from citizen scientist experts to expand the size of the dataset. In the future, we need to develop a web-based annotation tool to support collaboration with citizen scientist experts.

3 BASELINES ANALYSIS

In Section 1, we have introduced the four stages of ship detection, namely dividing an image into blocks, sea-land segmentation, candidate generation and ship classification. Dividing an image into blocks is necessary for space-based system. However, we assume that images in HRSC2016 dataset are blocks from large volume images. In the future, we will provide some large volume images to evaluate computing time for algorithms. In this section, we analyze other three stages on HRSC2016 dataset.

3.1 Sea-land Segmentation

Sea-land segmentation for ship detection can be divided into two stages including sea separation and land separation. In sea separation task, sea regions are separated from land and ship foregrounds by fast segmentation methods (You and Li, 2011; Liu et al., 2014; Tang et al., 2015). In land separation task, land regions are always masked by the land masks generated by geographic information (Zou and Shi, 2016) or removed by region classification methods (Tang et al., 2015) which is also called false alarm removing. However, HRSC2016 does not support evaluating land separation methods based on public geographic information because of Google Earth's geographic coordinate shift. In this section, we mainly focus on evaluating sea separation task also called sea-land segmentation in many works.
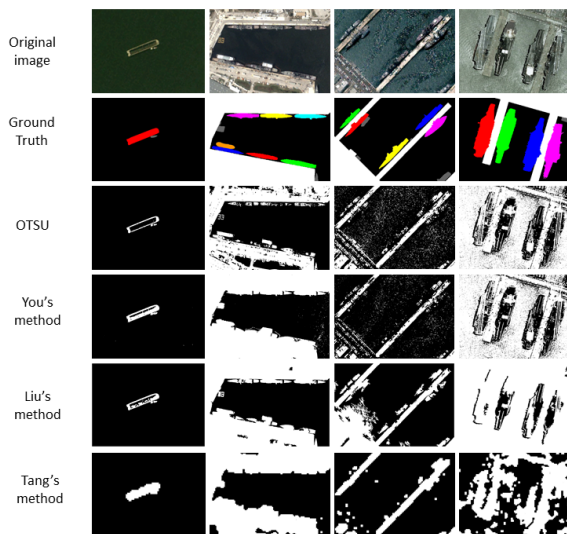
Figure 6: Samples of the sea-land segmentation results.

The authors of existing sea-land segmentation related works evaluated experimental performance by visual inspection which is subjective and coarse-grained. We need to design an evaluation criterion used for quantitative analysis.

The sea-land segmentation plays two roles in ship detection task. On the one hand, it can improve the computational efficiency by quickly removing the large sea regions to avoid computation. On the other hand, it can help to extract ships on sea. However, you should try your best to keep ship regions from being destroyed while removing sea regions. This requires the new evaluation criterion not only can evaluate the accuracy of sea separation, but also can measure the integrity of ships reserved.

We propose a metric called separation fitness (SF) to measure the performance of sea-land segmentation. We introduce the typically intersection over union (IoU) criterion to evaluate the accuracy of sea segmentation. Here IoU is used to compute the intersection of the candidate sea regions segmented and the ground truth sea regions divided by the area of their union. IoU value is between 0 and 1. We introduce ship integrity to measure the intactness of ship regions after segmentation. Then we define separation fitness as IoU multiplies ship integrity:

$$SF = \frac{A(S' \cap S)}{A(S' \cup S)} \times (1 - \frac{A(S'_o)}{A(O)}) \qquad (1)$$

where $A(.)$ is a function used to calculate the area, S' is the candidate sea region segmented, S is the ground truth sea region, O and S'_o are the ground truth ship regions and the overlaps between the candidate sea regions and the ground truth ship regions, respec-

Table 1: Evaluating baselines using separation fitness (SF).

	OTSU	You	Liu	Tang
Sea IoU	0.858	0.873	0.901	0.868
Ship integrity	0.656	0.839	0.828	0.944
SF	0.569	0.739	0.751	0.823
Avg Time (S)	0.023	0.447	0.317	0.026

tively. SF rewards both high accuracy and good ship integrity.

We select three state-of-the-art methods including You's method (You and Li, 2011), Liu's method (Liu et al., 2014) and Tang's method (Tang et al., 2015). In addition, we also choose OTSU (Otsu, 1975) method, that is often used as a comparison method, as one of our baselines. The samples of the experimental results can be seen in Figure 6 and the performance evaluation can be seen in Table 1. We can see that Liu's method has the highest Sea IoU, but much lower ship integrity than Tang's method. Tang's method has the highest ship integrity, the best SF and very short average computation time per image. However, from the last column in Figure 6, we can see that all these methods are difficult to deal with clutter sea.

3.2 Ship Candidate Generation

The purpose of ship candidate (proposal) generation is to locate ships. The ship candidates generated in this stage contains a lot of false alarms which will be further removed by strong classifiers followed. The state-of-the-art ship candidate generation methods had been compared on our dataset by Liu et al. (Liu et al., 2016) who proposed a method with the best performance based on ship rotated bounding box space (called SRBBS method for convenience). The baselines of ship candidate generation include the following methods:

- SRBBS method (Liu et al., 2016);
- BING based on SRBBS (Liu et al., 2016);
- Liu's method (Liu et al., 2014);
- Tang's method (Tang et al., 2015).

In this paper, we do not discuss these methods any more.

3.3 Ship Classification

In this section, we will build ship recognition baselines on the classification tasks of all the three levels of HRSC2016. After ship candidate generation, false alarms need to be further removed and the true positives need to be properly classified. In Section 1, we have introduced that most of the existing

Table 2: The 9 variants' mAP values in the level 1 task.

	REG-BB	REG-RBB	REG-BOTH
NBEB	0.797	0.784	0.773
NREB	0.791	0.790	0.780
NRER	0.557	0.696	0.681

Table 3: The AP and mAP values of the two baselines in the level 2 task.

	ship	air.	war.	mer.	mAP
BL1	0.451	0.844	0.872	0.741	0.727
BL2	0.451	0.510	0.752	0.639	0.588

methods only classified candidates into two classes, namely background and ship. Some methods identified ships by commonly Geometric features (Yang et al., 2014; Tang et al., 2015), such as compactness, Length-width ratio, etc. Shi et al. (Shi et al., 2014; Qi et al., 2015) designed some new improved handcrafted features based on HOG (Dalal and Triggs, 2005) feature. Recently, automatically learned features for ship detection based on Convolutional Neural Network(CNN) were used (Yu et al., 2015; Zou and Shi, 2016; Zhang et al., 2016). And HOG (Dalal and Triggs, 2005) combined with SVM is commonly used as a comparison method. However, experiments had shown that HOG has much weaker representative ability than CNN feature which achieves great successes in many computer vision problems. In order to promote the improvement of ship recognition, CNN features should be introduced into the ship recognition task as baselines.

The state of the art ship detection frameworks with deep CNN models as backbones include R-CNN (Girshick et al., 2014), Fast RCNN (Girshick, 2015) and Faster RCNN (Ren et al., 2015), etc. R-CNN model can be divided into two stages, namely region proposal generation and CNN feature extraction followed by classifiers that usually are Softmax Regression classifiers or linear SVMs. However, It is inefficient for R-CNN to perform feature extraction for each region independently, because the magnitude of the proposal number may be around 10^3. Fast RCNN, which is suitable for ship recognition, can greatly improve the efficiency by sharing convolutional computation before region of interest pooling (RoI pooling). Instead of independent method for region proposal generation, Faster RCNN generates candidate regions by a Region Proposal Network(RPN) model. The RPN together with an Object Detection Network are trained for sharing convolutional layers for fast computation. Faster RCNN has better performance and higher efficiency than Fast RCNN. However, it is inappropriate to introduce Faster RCNN directly into ship detection, because the RPN is not strong enough to deal with rotations and ship clusters. It will be further researched in the future.

Based on Fast RCNN framework, we select SRBBS method (Liu et al., 2016) as region proposal generation method and the AlexNet (Krizhevsky et al., 2012) as the backbone. In addition to the ex-

isting bounding box regression model (REG-BB), we design another 2 different region regression models for Fast RCNN, namely rotated bounding box regression model (REG-RBB) and bounding box together with rotated bounding box regression model (REG-BOTH). To regress rotated bounding box, we define the regression loss for REG-RBB model as

$$L_{loc}(t^u, v) = \sum_{i \in \{x,y,w,h,a\}} smooth_{L_1}(t_i^u - v_i), \quad (2)$$

$$smooth_{L_1}(x) = \begin{cases} 0.5x^2 & if\ |x| < 1 \\ |x| - 0.5 & otherwise \end{cases}, \quad (3)$$

$$t_x = (G_x - P_x)/(P_w \cos\theta + P_h \sin|\theta|), \quad (4)$$

$$t_y = (G_y - P_y)/(P_w \sin|\theta| + P_h \cos\theta), \quad (5)$$

$$t_w = \log(G_w/P_w), \quad (6)$$

$$t_h = \log(G_h/P_h), \quad (7)$$

$$t_a = (G_a - P_a)/(\lambda 180), \quad (8)$$

where u is the ground-truth class of a training RoI, $v = (v_x, v_y, v_w, v_h, v_a)$ is the ground-truth rotated bounding box regression target, $t^u = (t_x^u, t_y^u, t_w^u, t_h^u, t_a^u)$ is a predicted tuple, $P = (P_x, P_y, P_w, P_h, P_a)$ specifies the pixel coordinates of the center of proposal P's rotated bounding box together with P's width, height in pixels and rotation angle (between -90 and 90), θ is P_a, G is defined in the same way: $G = (G_x, G_y, G_w, G_h, G_a)$ and λ is a constant number ($\lambda = 0.5$). For REG-BOTH model, we design the loss function similar to Equation (2), but with t^u and v of 9 dimensions. In the test mode, after NMS between bounding box candidates, the Fast RCNN evaluates performance using the criterion IoU, that candidates with $IoU \geq 0.5$ are seen as true positive candidates, between a proposal's bounding box and the corresponding ground truth's bounding box. Besides this strategy (NBEB for short), we add another two strategies including evaluation by corresponding bounding box candidates after NMS on Rotated bounding box candidates (NREB) and evaluation by rotated bounding box candidates after NMS on them (NRER). By the combination of these three evaluation strategies with the three regression models, we get nine variants of Fast RCNN shown in Table 2.

Thanks to the RBB candidates from SRBBS method, we can get a series of corresponding proposals with both RBB and BB (minimum bounding rectangle of RBB) information. Benefiting from this,

Table 4: The two baselines' AP values in the level 3 task. BL1's and BL2's mAP values are 0.608 and 0.452 respectively.

class	BL1	BL2	class	BL1	BL2	class	BL1	BL2	class	BL1	BL2
ship	0.463	0.419	air.	0.844	0.412	mer.	0.355	0.128	war.	0.078	0.039
Arl.	0.778	0.710	Aus.	0.569	0.432	Car.A	0.804	0.531	Car.B	0.831	0.678
Com.A	0.643	0.571	Con.	0.465	0.368	Con.A	0.675	0.496	Ent.	0.229	0.030
Med.	0.887	0.788	Nim.	0.642	0.446	Per.	0.632	0.439	San.	0.535	0.514
Tar.	0.771	0.509	Tic.	0.746	0.574	Whi.	0.599	0.509			

we can also get both BB and RBB information for predicted candidates without BB or RBB regression information. In the classification experiments, we exclude submarine, hovercraft classes and samples with "difficult" label as Liu did in (Liu et al., 2016). We use the same pre-trained network as Fast RCNN method and select linear SVMs as classifiers. Using the 9 variants, We perform level 1 task of HRSC2016. The results are shown in Table 2. The IoU thresholds of NBEB, NREB and NRER for NMS are empirically set as 0.3,0.05 and 0.05 respectively. We use criteria average precision (AP) and mean average precision (mAP) (Girshick et al., 2014) to measure the performances. We can see that performances of variants with bounding box evaluation way are close. But when we perform evaluation on RBB candidates, the variants with the RBB regression model achieve much better performance. The variants with REG-BOTH model has close but lower mAP values than the ones with REG-RBB model. We also find that variants with RBB evaluation way has much lower mAP values than the ones with bounding box evaluation way. However, RBB labeling way can provide more accurate bounding information. In this paper, from the nine variants, we select NBEB combined with REG-BB method and NRER combined with REG-RBB method as our baselines respectively called as the following:

- SRBBS-Fast-RCNN (BL1);

- SRBBS-Fast-RCNN-R (BL2).

The two baseline methods also apply to the level 2 and level 3 tasks of HRSC2016. The experimental results are shown in Table 3 and Table 4. Due to the reduction in the number of each class and the shorter distances between classes, we got worse performances on the level 2 and level 3 tasks. It can be found that the finer the granularity of recognition, the worse the performance is. It is worth noting that it is a big challenge to recognize higher level classes, such as ship, warcraft, etc, in level 3 task, because distances between samples in a higher level class may be much longer than distances between samples with different classes.

4 CONCLUSIONS

In this paper, we wish to promote the field of ship recognition by optical remote sensing images, which is getting more and more attention. We introduced a high resolution optical remote sensing dataset for ship recognition, namely HRSC2016. To the best of our knowledge, this is the first public remote sensing dataset for ship recognition. We analyzed several unique features of HRSC2016, including ship hierarchy, an abundance of bounding information, unbiasedness and rich helping tools, etc. We also performed a detailed analysis of the state of the art methods on HRSC2016. For sea-land segmentation, we introduced a novel metric SF to measure the performance. For ship classification, we proposed some new baselines based on deep CNN features and performed them on the three level ship recognition tasks of HRSC2016. There are still many challenges about ship recognition including the problem about how to recognize ships in a cluster, the problem of ship recognition with small number of samples and the problem about rotated RoI pooling, etc.

In the future, we will further extent HRSC2016 in the help of citizen scientist experts and build more baselines, for example, the HOG feature combined with SVMs, the SRBBS method combined with RCNN model and variants of Faster-RCNN, etc.

ACKNOWLEDGEMENTS

REFERENCES

Corbane, C., Najman, L., Pecoul, E., Demagistri, L., and Petit, M. (2010). A complete processing chain for ship detection using optical satellite imagery. *International Journal of Remote Sensing*, 31(22):5837–5854.

Corbane, C. and Petit, M. (2008). Fully automated procedure for ship detection using optical satellite imagery.

Proceedings of SPIE - The International Society for Optical Engineering, 7150(10):2752–65.

Dalal, N. and Triggs, B. (2005). Histograms of oriented gradients for human detection. In *Proc. IEEE Int. Conf. Comput. Vis. Pattern Recognit.*, volume 1, pages 886–893. IEEE.

Gan, L., Liu, P., and Wang, L. (2015). Rotation sliding window of the hog feature in remote sensing images for ship detection. In *2015 8th International Symposium on Computational Intelligence and Design (ISCID)*, volume 1, pages 401–404. IEEE.

Girshick, R. (2015). Fast r-cnn. In *Proc. IEEE Int. Conf. Comput. Vis.*, pages 1440–1448.

Girshick, R., Donahue, J., Darrell, T., and Malik, J. (2014). Rich feature hierarchies for accurate object detection and semantic segmentation. In *Proc. IEEE Int. Conf. Comput. Vis. Pattern Recognit.*, pages 580–587.

Guo, W., Xia, X., and Wang, X. (2014). A remote sensing ship recognition method based on dynamic probability generative model. *Expert Systems with Applications*, 41(14):6446–6458.

Han, J., Zhang, D., Cheng, G., Guo, L., and Ren, J. (2015). Object detection in optical remote sensing images based on weakly supervised learning and high-level feature learning. *IEEE Trans. Geosci. Remote Sens.*, 53(6):3325–3337.

Krizhevsky, A., Sutskever, I., and Hinton, G. E. (2012). Imagenet classification with deep convolutional neural networks. In *Advances in neural information processing systems*, pages 1097–1105.

Liu, G., Zhang, Y., Zheng, X., Sun, X., Fu, K., and Wang, H. (2014). A new method on inshore ship detection in high-resolution satellite images using shape and context information. *IEEE Geosci. Remote Sens. Lett.*, 11(3):617–621.

Liu, P. (2015). A survey of remote-sensing big data. *Frontiers in Environmental Science*, 3:45.

Liu, Z., Wang, H., Weng, L., and Yang, Y. (2016). Ship rotated bounding box space for ship extraction from high-resolution optical satellite images with complex backgrounds. *IEEE Geosci. Remote Sens. Lett.*, 13(8):1074–1078.

Otsu, N. (1975). A threshold selection method from gray-level histograms. *Automatica*, 11(285-296):23–27.

Proia, N. and Page, V. (2010). Characterization of a bayesian ship detection method in optical satellite images. *IEEE Geosci. Remote Sens. Lett.*, 7(2):226–230.

Qi, S., Ma, J., Lin, J., and Li, Y. (2015). Unsupervised ship detection based on saliency and s-hog descriptor from optical satellite images. *IEEE Geosci. Remote Sens. Lett.*, 12(7):1–5.

Ren, S., He, K., Girshick, R., and Sun, J. (2015). Faster r-cnn: Towards real-time object detection with region proposal networks. In *Advances in neural information processing systems*, pages 91–99.

Shi, Z., Yu, X., Jiang, Z., and Li, B. (2014). Ship detection in high-resolution optical imagery based on anomaly detector and local shape feature. *IEEE Trans. Geosci. Remote Sens.*, 52(8):4511–4523.

Tang, J., Deng, C., Huang, G. B., and Zhao, B. (2015). Compressed-domain ship detection on spaceborne optical image using deep neural network and extreme learning machine. *IEEE Trans. Geosci. Remote Sens.*, 53(3):1174–1185.

Van Horn, G., Branson, S., Farrell, R., Haber, S., Barry, J., Ipeirotis, P., Perona, P., and Belongie, S. (2015). Building a bird recognition app and large scale dataset with citizen scientists: The fine print in fine-grained dataset collection. In *Proc. IEEE Int. Conf. Comput. Vis. Pattern Recognit.*, pages 595–604.

Xu, J., Sun, X., Zhang, D., and Fu, K. (2014). Automatic detection of inshore ships in high-resolution remote sensing images using robust invariant generalized hough transform. *IEEE Geosci. Remote Sens. Lett.*, 11(12):2070–2074.

Yang, G., Li, B., Ji, S., Gao, F., and Xu, Q. (2014). Ship detection from optical satellite images based on sea surface analysis. *IEEE Geosci. Remote Sens. Lett.*, 11(3):641–645.

Yang, L., Luo, P., Change Loy, C., and Tang, X. (2015). A large-scale car dataset for fine-grained categorization and verification. In *Proc. IEEE Int. Conf. Comput. Vis. Pattern Recognit.*, pages 3973–3981.

Yang, Y. and Newsam, S. (2010). Bag-of-visual-words and spatial extensions for land-use classification. In *Proceedings of the 18th SIGSPATIAL international conference on advances in geographic information systems*, pages 270–279. ACM.

Yokoya, N. and Iwasaki, A. (2015). Object detection based on sparse representation and hough voting for optical remote sensing imagery. *IEEE Journal of Selected Topics in Applied Earth Observations & Remote Sensing*, 8(5):1–1.

You, X. and Li, W. (2011). A sea-land segmentation scheme based on statistical model of sea. In *International Congress on Image and Signal Processing*, pages 1155–1159.

Yu, Y., Guan, H., and Ji, Z. (2015). Rotation-invariant object detection in high-resolution satellite imagery using superpixel-based deep hough forests. *IEEE Geosci. Remote Sens. Lett.*, 12(11):2183–2187.

Zhang, R., Yao, J., Zhang, K., Feng, C., and Zhang, J. (2016). S-cnn ship detection from high-resolution remote sensing images. *ISPRS - International Archives of the Photogrammetry, Remote Sensing and Spatial Information Sciences*.

Zhu, C., Zhou, H., Wang, R., and Guo, J. (2010). A novel hierarchical method of ship detection from spaceborne optical image based on shape and texture features. *IEEE Trans. Geosci. Remote Sens.*, 48(9):3446–3456.

Zou, Z. and Shi, Z. (2016). Ship detection in spaceborne optical image with svd networks. *IEEE Trans. Geosci. Remote Sens.*, 54(10):5832–5845.